Research Article

Dynamic Prediction Model of Multisource Gas Emissions in a Fully Mechanized Top Coal Caving Based on the Coal Particle Size Distribution

Han Gao,[1,2] Xuanping Gong,[2] Xiaoyu Cheng ⓘ,[2] and Rui Yu[3]

[1]*Beijing Key Laboratory for Precise Mining of Intergrown Energy and Resource,*
China University of Mining and Technology (Beijing), Beijing 100083, China
[2]*China Coal Energy Research Institute Co., Ltd., Xi'an 710054, China*
[3]*China Coal Hua Jin Group Co., Ltd., He Jin 043300, China*

Correspondence should be addressed to Xiaoyu Cheng; chengxiaoyu89@126.com

Coal particle size is an important factor affecting the gas emission law. Taking Wangjialing coal mine as the research object, the particle size distribution of coal mining and caving is analyzed via field tests in order to develop the gas emission theoretical model from granular coal. We also perform the numerical simulation of the coal body and longwall face gas emission characteristics under different particles. Finally, the gas emission rules of coal cutting, caving, longwall face, and goaf in Wangjialing coal mine are analyzed, and the dynamic prediction model, which accounts for the time influence of the coal cutting and coal caving speed based on the particle size distribution characteristics, is derived. Results demonstrate the wide distribution of the coal particle size at Wangjialing coal mine, with a higher proportion of small- and large-sized particles. The smaller the coal particle size, the faster the gas emission and the smaller the desorption ratio of coal at ≥ 20 mm within 30 min. The comprehensive emission intensity of coal mining and caving can be described by an exponential function. The initial emission intensity of coal mining is observed to exceed that of coal caving, while the attenuation laws of the two are essentially equal, and the majority of the gas emission is completed within 5 min. The error between the results of the multisource dynamic prediction model and the field measurement is small, which is of practical application significance.

1. Introduction

The targeted control of mine gas requires the accurate determination of the gas emission quantity and the gas emission law during the mine production process [1–3]. The source separation prediction method is the most commonly used approach for predicting the amount of gas emitted in production mines. However, due to the inhomogeneity of gas emissions, mines that do not exhibit gas exceeding limits via the source separation prediction method may also present local exceeding limits, instantaneous exceeding limits, and other problems in actual production [4–8].

Numerous computer-based prediction methods have been proposed over the years [9–14]. Fu et al. [15] developed a dynamic prediction method of absolute gas emissions based on the Elman neural network optimized by the ant colony clustering algorithm. By integrating historical mine data, the authors established a prediction model of absolute gas emissions based on the acc-enn algorithm. Liu et al. [16] proposed an enhanced cart regression algorithm based on a support vector machine due to its ability to model the output of each leaf node. Based on the seepage mechanics method, Zhang et al. [17] derived a formula to predict gas emissions in the heading face and discussed the accuracy of the predicted value during the field excavation process. Lv et al. [18] obtained the key factors affecting the gas emission of the working face via principal component analysis, which were then employed for a multistep linear regression to predict the gas emission of the working face. Zhu et al. [19] established a gas emission prediction model for the mining

coal seam, adjacent coal seam, and goaf based on a neural ne twork and applied it to an actual mine.

The particle size of coal is considered as an important factor affecting gas desorption, except for water and temperature [20–29]. In order to investigate the desorption diffusion characteristics of gas bearing coal under pressure, Li et al. [30] established a dynamic evolution model of the gas diffusion coefficient of loaded coal and calculated the vas diffusion coefficient of coal samples with particle sizes of 0.25–0.5, 0.5–1, and 1–2 mm under the axial pressure of 0–12 MPa, based on a single and double pore model. Kang et al. [31] applied a self-designed lump coal adsorption/desorption experimental device to study the CH_4 isothermal adsorption/desorption characteristics of lump coal with the same volume of primary structure, cataclastic coal, and mylonite coal under low pressure and discussed the influence of the coal structure on CH_4 adsorption/desorption. Liu et al. [32] examined the quantitative relationship between gas diffusion flux and temperature of coal particles under different ranks. They determined the correction method and regression coefficient of gas emission with temperature, as well as the quantitative variation law of the gas diffusion coefficient with increasing coal particle temperatures across different ranks.

Despite the great progress made by previous research on gas emission predictions, there is still room for development. In terms of gas emission predictions, the current separate source prediction method is not suitable for fully mechanized top coal caving mining conditions, while prediction methods based on mathematical models do not fully consider the key influencing factors and time dynamic effect of gas emission, and thus, the results cannot accurately guide the field practices. Moreover, the majority of studies on the key influencing factors of gas emission focus on the gas desorption law under the conventional standard coal particle size, ignoring the actual coal particle size distribution in the field. In the actual production process, the nonuniform coal particle size will inevitably have an impact on the gas emission law. For the fully mechanized top coal caving mining method, research on the difference between the gas emission law of coal mining and caving is limited, and the dynamic prediction model based on these laws considering the coal caving and coal wall exposure time also requires work.

In this paper, we select Wangjialing coal mine as the research object to test the particle size distribution of the fully mechanized caving face via image recognition and statistical methods. Furthermore, numerical simulations are performed to investigate the gas desorption law under the coal particle size distribution and to determine the variations in gas emission intensity. The dynamic prediction model of multisource gas emission in a fully mechanized top coal caving mining is then mathematically derived considering the key factors of gas emission. We verify the model by field data. Our work provides a basis for the prediction, law, and control of gas emission in fully mechanized mining, particularly caving mining.

The principle coal seam of Wangjialing coal mine is a No. 2 coal seam, with a mining height of 6 m. The original gas content of the coal seam is only 3.19–5.41 m^3/t, indicating a typical gas mine with high gas content caused by high

strength mining in a low gas coal seam. Key gas sources include coal cutting, coal caving, longwall face, and goaf.

2. Materials and Methods

2.1. Coal Size Distribution Measurements in a Fully Mechanized Workface. The particle size distribution exerts a great influence on the gas emission law of coal falling, and thus, the actual particle size distribution of coal falling should be determined through testing. Wangjialing coal mine adopts the comprehensive caving method. The caving coal is broken by the shearer drum, while during caving, the caving coal is broken naturally. The crushing methods required for both processes are distinct, and therefore, the particle size distribution of coal caving and caving should be analyzed separately.

The equipment used in the particle size distribution tests include a mine explosion-proof camera, camera overhead frame, explosion-proof fill light, and ruler. The testing process is described in the following. The camera was fixed with the overhead frame, placing the ruler flat above the falling coal (Figure 1), using the overhead frame to keep the camera line of sight perpendicular to the coal body and to minimize the imaging deformation during the shooting process. The coal mining (front scraper) and coal caving (rear scraper) in the Wangjialing 12322 face were photographed separately. The collected images were then analyzed in the laboratory. Image Pro Plus was applied to analyze the particle size of coal in the image, with the length of A4 paper (297 mm) as the measuring scale. Based on this, the unit of the scale was set and generated, and the measurement range was adjusted via a mouse on the image. The values required to measure the coal particle size were then automatically generated (Figures 1 and 2).

In order to avoid measurement errors, field tests were repeated four times on May 20, May 26, August 12, and August 17, 2019. The average measurements of the four tests were employed to plot the histogram of the particle size distribution (mass ratio) for the front scraper and rear scraper coal bodies (Figures 3 and 4, respectively). The grain size of the coal cutting and coal caving is observed to lie within 20–60 mm, with coal mining and coal caving accounting for 52.1% and 69.8%, respectively. The proportion of coal taken at 0–20 mm (18.5%) exceeds that of the discharged coal (7.3%), while the 60–100 mm mining falling coal (20.3%) and caving coal (22.1%) both have the second largest proportion, and the proportion of caving coal (0.8%) above 100 mm is minimal. The grain size distribution of coal mining is more dispersed than that of coal caving and also exhibits a higher proportion of small- and large-sized particles. These differences may be related to different coal breaking methods.

2.2. Gas Emission Intensity of the Coal Particle/Body

2.2.1. Theoretical Model of Coal Gas Emission. As described in Section 1, coal particle gas adsorption and atmospheric emptying experiments are commonly used to test coal particle gas emissions in the laboratory. However, the time required to reach a gas adsorption equilibrium for large-scale coal particles increases exponentially with the number
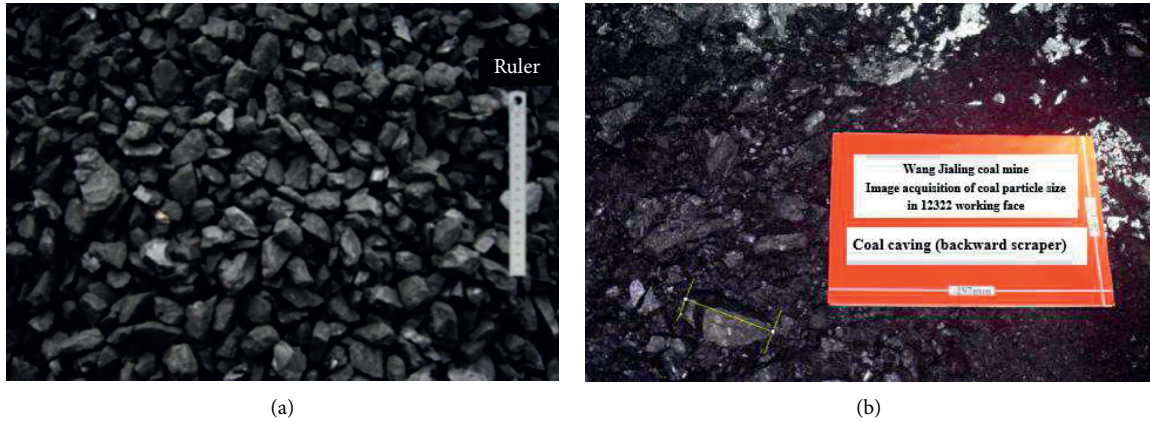
(a)

(b)

FIGURE 1: Measuring process of coal particle size. (a) Field shooting and ruler placement. (b) Coal size measurement.
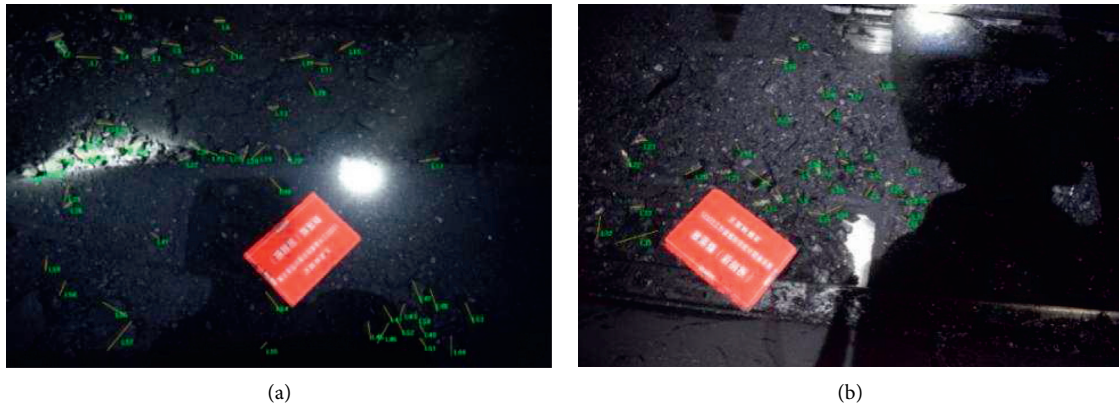

(a)

(b)

FIGURE 2: Test image processing. (a) Particle size image analysis of front scraper coal. (b) Particle size image analysis of backward scraper coal.
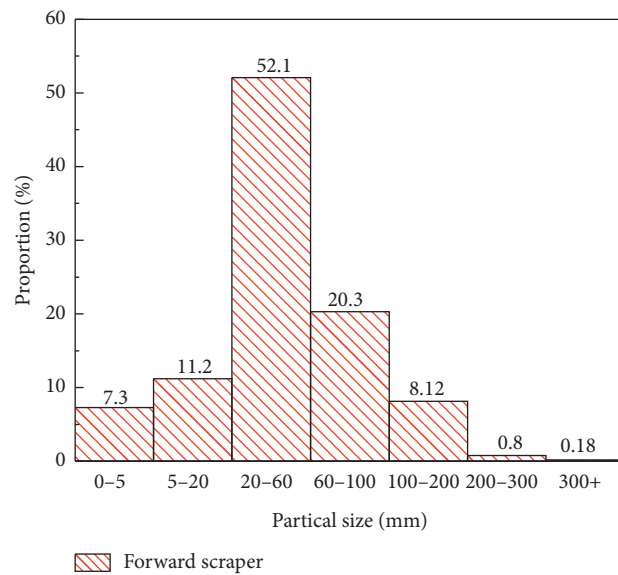

FIGURE 3: Histogram of coal particle size in coal mining (forward scraper).
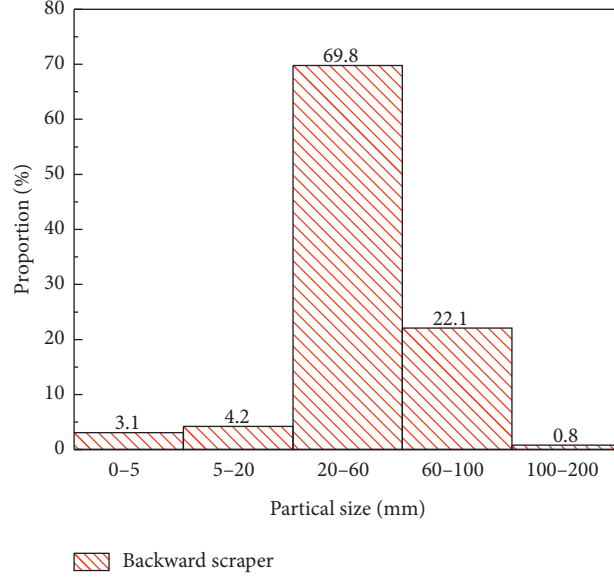
FIGURE 4: Histogram of coal particle size in coal caving (backward scraper).

of coal particles or even more than a few months. Thus, we adopt numerical calculations to determine the coal particle gas emission theoretical model.

The relationship between the free gas pressure and gas concentration can be calculated using the ideal gas state equation:

$$C = \frac{p}{ZRT}, \tag{1}$$

where p is the gas pressure, Z is the gas compression factor, R is the gas constant, and T is the experimental temperature.

Moreover, the gas adsorption law can be determined using Lang's adsorption equation:

$$V_a = \frac{V_0 p}{P_L + p}, \tag{2}$$

where V_a is the gas adsorption volume, V_0 is Lang's adsorption capacity, and P_L is Lang's adsorption pressure.

For each unit volume of coal particles, the total amount of gas adsorption is taken as

$$m_m = m_a + m_f, \tag{3}$$

where m_a is the mass of the adsorbed gas and m_f is the mass of the free gas in the coal body pore, and is calculated as follows:

$$m_a = V_a \rho_c \rho_{sg},$$
$$m_f = \frac{\Phi p M}{ZRT}, \tag{4}$$

where ρ_c is the density of granular coal, ρ_{sg} is the standard state gas density, Φ is the coal porosity, and M is the molar mass of gas. Thus, m_m can be expressed as

$$m_m = \frac{V_0 ZRTC}{P_L + ZRTC} \rho_c \rho_{sg} + \Phi C M. \tag{5}$$

For a unit coal body, during the gas emission process, the amount of diffused gas emission is equal to the change of gas content in the coal body. According to the law of mass conservation and the law of Fick diffusion, we have

$$\frac{\partial m_m}{\partial t} + \nabla \cdot (-DM\nabla C) = 0. \tag{6}$$

The gas diffusion and emission in unit particles can then be obtained as follows:

$$\frac{V_0 P_L ZRT \rho_c \rho_{sg}}{(P_L + CZRT)^2} \frac{\partial C}{\partial t} + \frac{\Phi M}{ZRT} \frac{\partial C}{\partial t} + \nabla \cdot (-DM\nabla C) = 0. \tag{7}$$

The geometry of the simulation object is subsequently established in the numerical simulation software, and the boundary conditions and initial conditions are given as

$$\begin{cases} C = C_f, \\ \nabla C \vec{n} = 0 \end{cases} \text{ on } \partial\Omega, \tag{8}$$
$$C = C_0 \text{ in } \partial\Omega,$$

where Ω is the particle coal boundary, C_f is the variation law of the gas pressure outside the coal, to the actual situation on the spot, and $C_f = 0.1$ MPa. At t, the gas mass emitted from the granular coal is equal to the volume fraction of the gas mass in all unit coal bodies:

$$M_t = \int\int\int \left(\frac{V_0 ZRTC}{P_L + ZRTC} \rho_c \rho_{sg} + \Phi C M \right) \Big|_t. \tag{9}$$

2.2.2. *The Law and Strength of Coal Grain Gas Emission.* Based on the theoretical model derived in the previous section, COMSOL Multiphysics is used to simulate the gas emission law of coal under different particle sizes. The shape of the coal particle is taken as a cube, and the size is taken as

the intermediate value of each particle size range. Table 1 reports the parameters used in the numerical simulation, selected from the real parameters of Wangjialing coal mine to ensure the accuracy of the calculation results.

The residence time of falling coal in the working face does not typically exceed 30 min; thus, we take 1800 s as the simulation time period to analyze the changes in coal particle gas content and gas emission. In order to facilitate the analysis procedure, we select five horizontal sections of the coal particle gas content. We initially compare the variations in gas content at 10, 20, and 30 min for 0–5, 5–20, and 20–60 mm coal particles (Figure 5). The majority of the gas in the 0–5 mm coal particles is desorbed and gushed at 10 min, while for the 5–20 mm particles, this does not occur until 30 min. The gas content in some areas of the 20–60 mm coal particles remains unchanged during the whole transportation process, with the exception of very few areas near the surface. The results indicate that, as the coal particle size increases, the gas emission is directly related to the specific surface area of the coal, and the larger the scale, the smaller the gas emission.

Figure 6 presents the relationship between the gas emission intensity and time across different coal particle sizes, where each curve is fitted by the appropriate model.

Although the shape of the gas emission intensity varies slightly with time, all curves are fitted using the exponential function $y = \alpha \cdot \exp^{-\beta t} \gamma$, demonstrating correlation coefficients above 0.9 (Table 2). The smaller the particle size of the coal body, the larger the value of α and γ, indicating that initial increases of α are enhanced with the decreasing coal particle size, while β decreases with the coal particle size, indicating the increase in the gas emission attenuation rate.

2.2.3. The Law and Strength of Gas Emission in the Longwall Face of a Fully Mechanized Caving Face. Based on the theoretical model derived in Section 2.2.1, COMSOL Multiphysics is employed to simulate the dynamic emission law of the longwall face gas with exposure time in a fully mechanized caving face. In addition, a longwall face with a unit length of 4 m is established. The coal wall height is 3 m, and the top coal span is 5 m. The exposed longwall face is divided into the head-on longwall face and top longwall face. Figures 7 and 8 present the simulation process and calculation results, respectively.

The amount of gas emitted in the longwall face is generally observed to decrease as time increases. At the early stage of exposure, the decrease rate is steep and subsequently stabilizes in the later period. The fitting equation of the longwall face gas emission curve is determined as $V = 1.90764e^{-0.0023t} + 0.50677$, with a correlation coefficient R^2 of 0.99978.

3. Results

3.1. Prediction Model of Gas Emission from Coal Mining. The amount of coal gas emitted is generally a function of the coal quantity, analytical strength and exposure duration, and time of exposure. There is a clear relationship between the analytical strength and the particle size and exposure time of coal during the fully mechanized caving mining process, which can be described as

$$Q_c = \int_0^{t_c} \mathrm{d}V_c \cdot M_c, \tag{10}$$

where $\mathrm{d}V_c$ is the gas emission intensity at $\mathrm{d}t$ time for coal caving at different particle sizes, M_c is the coal mining weight, and t_c is the time of coal transportation, that is, the time when the coal falling body is transported out of the working face through the scraper conveyor and the belt.

Based on the gas emission intensity equation under different particle sizes and the proportion of different particle sizes in coal mining, we can conclude that

$$\mathrm{d}V = \left[f_1\left(\alpha_1 e^{-\beta_1 t} + \gamma_1\right) + f_2\left(\alpha_2 e^{-\beta_2 t} + \gamma_2\right) \right. \\ \left. + f_3\left(\alpha_3 e^{-\beta_3 t} + \gamma_3\right) + f_4\left(\alpha_4 e^{-\beta_4 t} + \gamma_4\right) + f_5\left(\alpha_5 e^{-\beta_5 t} + \gamma_5\right) \right]\mathrm{d}t, \tag{11}$$

where $\alpha/\beta/\gamma$ is the coal gas emission coefficient at different particle sizes based on the fitted curves of the gas emission intensity with time, t is the time of gas released in coal mining, and f is the distribution of coal across different particle sizes:

$$M_c = h_c \rho d v_c, \tag{12}$$

where h_c is the working face mining height, ρ is the coal density, d is the shearer cutting depth, and V_c is the coal cutting speed.

Equation (11) can be simplified based on the relationship between gas emission intensity and time of different ratio and particle size before. This allows us to calculate the strength of the combined gas emission of each particle size for $t = 0, 1, 2, 3, ..., 30$ min. Figure 9 presents the relationship between the time and intensity of comprehensive gas emissions. By fitting at the origin, the equation of t and V can be obtained as follows:

$$V_c = \alpha e^{-\beta t} + \gamma, \tag{13}$$

where $\alpha/\beta/\gamma$ is the coefficient of comprehensive gas emissions from coal mining, with $\alpha = 0.02849$, $\beta = 0.98023$, and $\gamma = 0.00265$.

The integral of t can be determined by substituting equations (12) and (13) into equation (10):

$$Q_c = h_c \rho d v_c \left[\frac{\alpha}{\beta}\left(1 - e^{-\beta t_c}\right) + \gamma t_c \right]. \tag{14}$$

3.2. Prediction Model of Gas Emission from Coal Caving. In fully mechanized caving mining, the gas emission equation for caving coal is consistent with that of coal mining:

$$Q_f = \int_0^{t_f} \mathrm{d}V_f \cdot M_f, \tag{15}$$

where $\mathrm{d}V_f$ is the gas emission intensity of coal caving at $\mathrm{d}t$ under different particle sizes, M_f is the weight of the coal caving, and t_f is the time to transport caving, that is, the time spent when the coal caving is transported out of the working face through the scraper conveyor and the belt. In particular,

TABLE 1: Gas foundation parameters of Wangjialing coal mine.

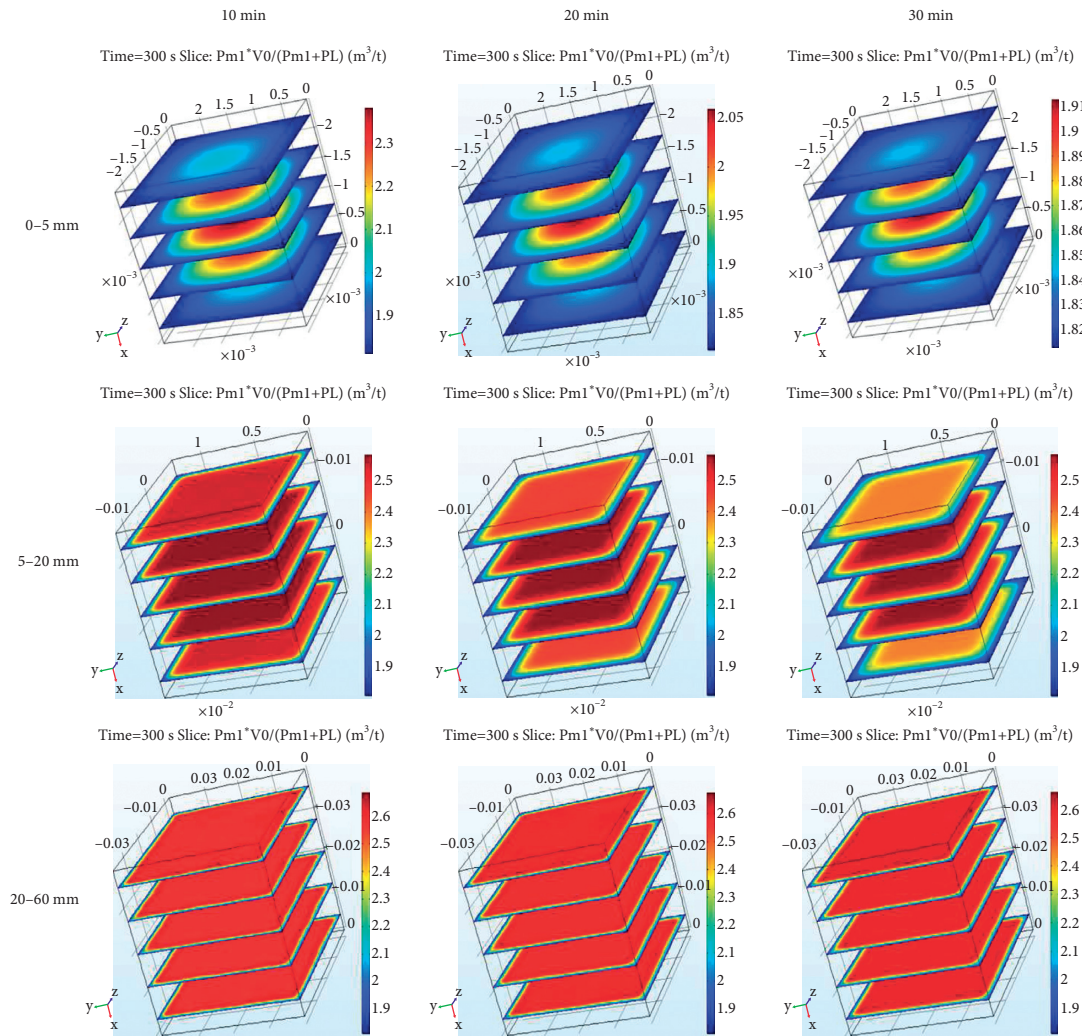| Parameter	Value
Lang's adsorption capacity	$29.2E^{-3}$ m^3/kg
Lang's adsorption pressure	0.95 MPa
Gas diffusion coefficient	$1.52E^{-10}$ m^2/s
Porosity of coal	4.2%
Parameter	Value
Coal density	$1.41E^3$ kg/m^3
Temperature	21°C
Original gas pressure	0.19 MPa
Original gas content	4.86 m^3/t

FIGURE 5: Variations in the gas content at the coal grain.

$$M_f = dv_f\rho\left[h_f - h_z(1-R)\right], \quad (16)$$

where h_f is the coal caving height, h_z is the total mining height, R is the recovery rate, ρ is the coal density, d is the coal caving step, that is, the shearer cutting depth, and V_f is the coal cutting speed.

Figure 10 presents the relationship between the time and intensity of the comprehensive gas emission based on the calculations in Section 3.1. The relationship between V, t, and coal under different particle sizes for comprehensive gas emissions can be described as follows:
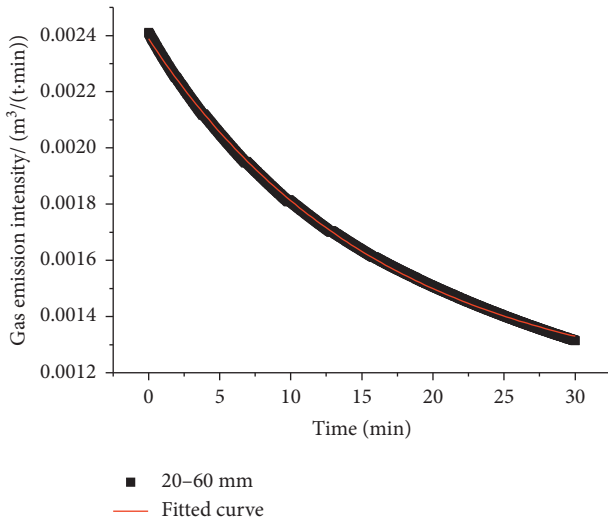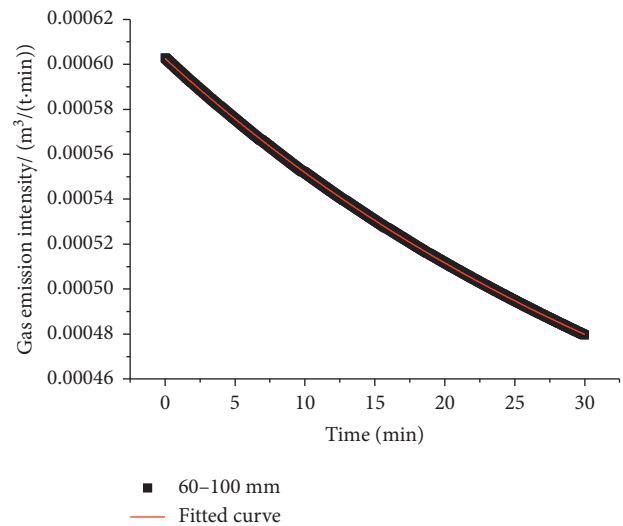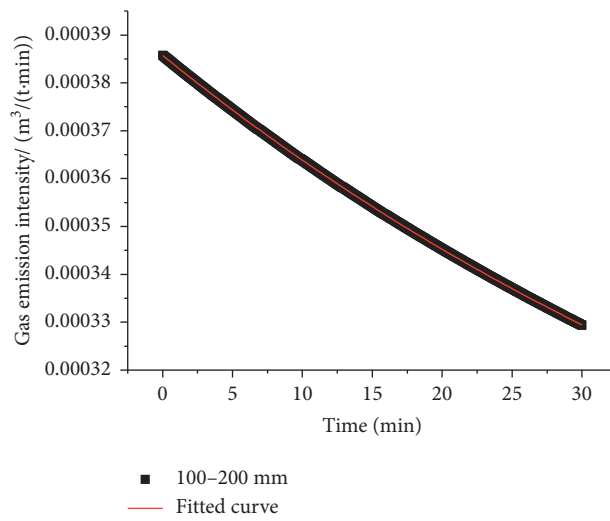
$$V_f = \alpha e^{-\beta t} + \gamma, \quad (17)$$
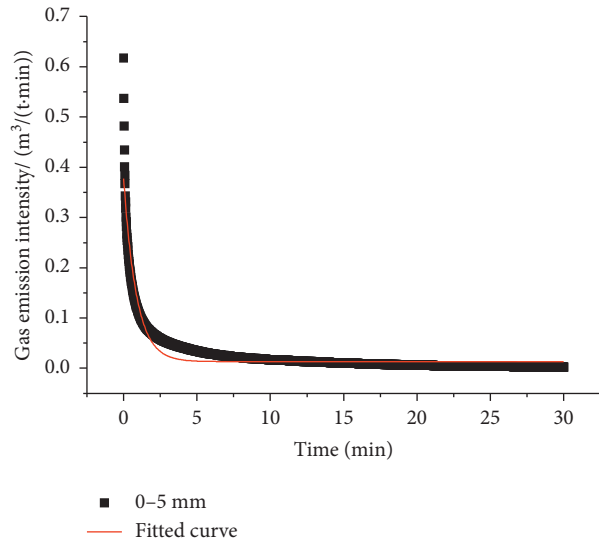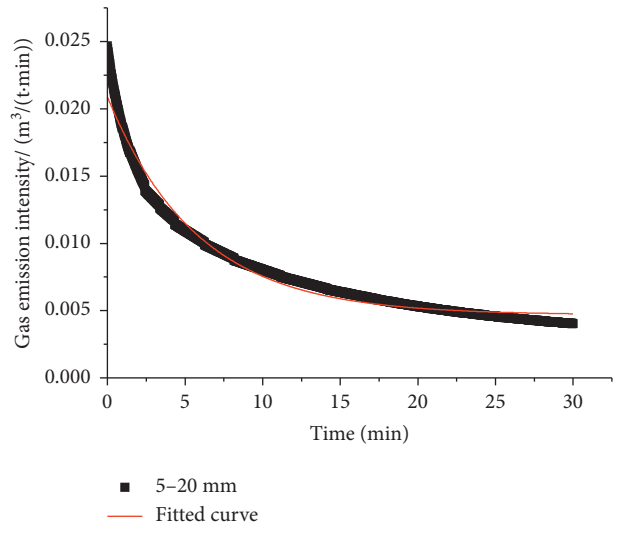
FIGURE 6: Variations in the gas desorption intensity with time and fitting results of coal across different grain sizes. (a) 0–5 mm. (b) 5–20 mm. (c) 20–60 mm. (d) 60–100 mm. (e) 100–200 mm.

TABLE 2: Fitting equations of the gas desorption strength curve for coal particle size.

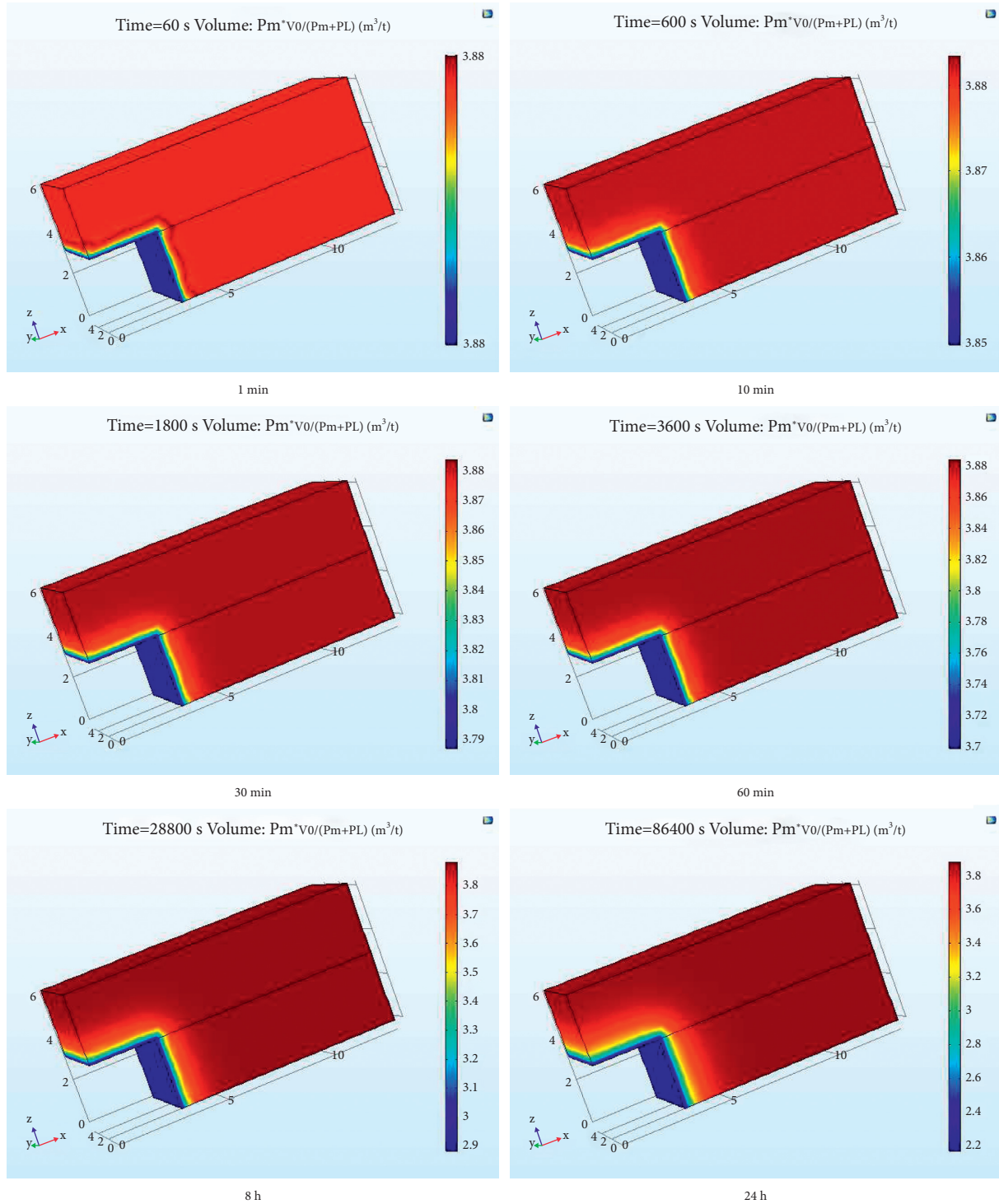| Particle size (mm)	Fitting equation	Correlation coefficient R^2
0–5	$V = 0.36446e^{-(-t/0.86571)} + 0.01309$	0.90
5–20	$V = 0.01619e^{-(-t/5.78089)} + 0.00468$	0.97
20–60	$V = 0.00126e^{-(-t/16.35778)} + 0.00113$	0.99
60–100	$V = 0.00023e^{-(-t/42.62183)} + 0.00036$	0.99
100–200	$V = 0.00006e^{-(-t/126.05799)} + 0.00011$	0.99

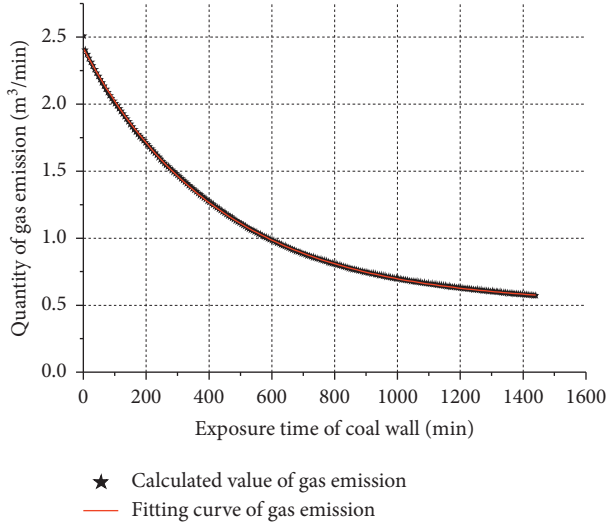FIGURE 7: Variations in the of gas content of coal.

FIGURE 8: Variations in the gas desorption intensity with time and fitting results.
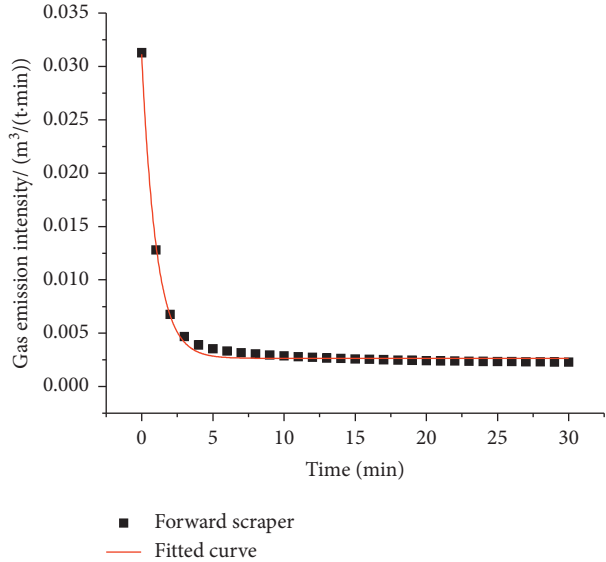

FIGURE 9: Relationship between coal mining time and comprehensive gas emission intensity.

where $\alpha/\beta/\gamma$ is the comprehensive gas emission coefficient of coal caving, with $\alpha = 0.01235$, $\beta = 0.9145$, and $\gamma = 0.00193$.

Equations (16) and (17) can be substituted into equation (15) to obtain integral t as follows:

$$Q_f = \left[\frac{\alpha}{\beta}\left(1 - e^{-\beta t_f}\right) + \gamma t_f\right]\rho d v_f\left[h_f - h_z(1 - R)\right]. \quad (18)$$

3.3. Prediction Model of Gas Emission in Goaf. In order to investigate the gas emission law and corresponding prediction model of a fully mechanized caving face, we make the following assumptions: (1) the residual coal is uniformly distributed in the goaf; (2) the coal left in the goaf is the left-over caving coal; (3) the gas source of the goaf in the working
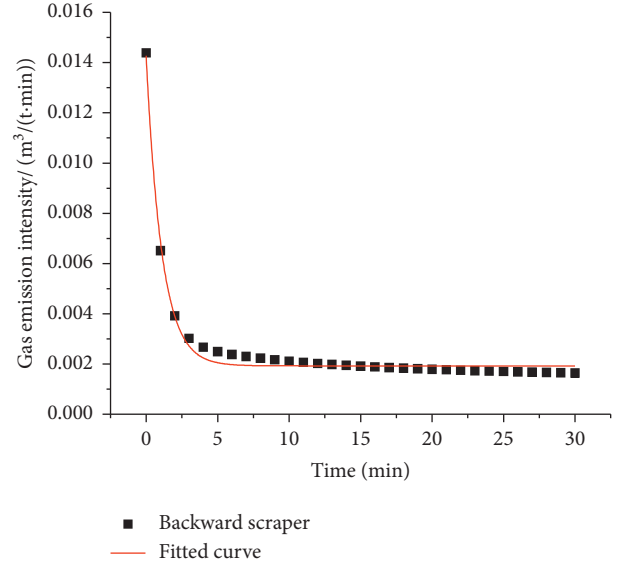

FIGURE 10: Relationship between caving time and comprehensive gas emission intensity.

face is the gas released by the coal left in a pressure cycle; (4) the ratio of the gas emission in the goaf to the total gas emission in the goaf under the same mining conditions is fixed.

The effective gas reserves in the goaf can be described as

$$Q_c = \int_0^t dV \cdot M_y, \quad (19)$$

where Q_c is the effective gas reserves in the goaf, dV is the gas emission intensity of coal with different particle sizes, M_y is the coal retention, and t is the coal exposed duration in the goaf.

Assumption (2) considers the coal left in the goaf to be the coal left from the caving coal, and thus, equation (11) can be used to derive the gas emission intensity under different particle sizes as follows:

$$V_y = \alpha e^{-\beta t} + \gamma, \quad (20)$$

where $\alpha/\beta/\gamma$ is the comprehensive gas emission coefficient of coal caving, with $\alpha = 0.01235$, $\beta = 0.9145$, and $\gamma = 0.00193$. In particular, we have

$$M_y = (1 - R)l_0 h_z \rho l, \quad (21)$$

where l_0 is the length of the working face and l is the propulsion distance of the working face within a pressure cycle. By substituting equations (20) and (21) into equation (19), the integral of t can be obtained:

$$Q_c = \left[\frac{\alpha}{\beta}\left(1 - e^{-\beta t}\right) + \gamma t\right](1 - R)l_0 h_z \rho l. \quad (22)$$

Based on the drainage measures adopted by Wangjialing mine for goaf gas and assumption (4), the proportion of goaf gas emissions to the total goaf gas emissions is fixed under the same mining conditions. This fixed proportion is denoted as θ, and the gas emission factor is as follows:

$$Q_{\mathrm{k}} = \theta(Q_{kz} - Q_c) = \theta\left[\frac{\alpha}{\beta t}\left(1 - e^{-\beta t}\right) + \gamma\right](1 - R)l_0 h_z \rho l - \theta Q_{\mathrm{c}},$$

$$(23)$$

where Q_c is the total gas extraction in the goaf and θ is the proportional factor of the gas emission, that is, the gas emission percentage from the goaf to the total gas release (excluding drainage) in the goaf.

3.4. Gas Emission Prediction Model for the Longwall Face. Based on the simulation results in Section 3.3, the coal wall gas emissions in a fully mechanized caving face can be described as

$$V = \alpha e^{-\beta t} + Y,$$

$$(24)$$

where t and $\alpha/\beta/\gamma$ are the exposed time and gas emission coefficient of the longwall face, respectively, with $\alpha = 1.9$, $\beta = 0.0023$, and $\gamma = 0.5$.

Considering the time effect in the gas emission process from the longwall face, combined with the initial numerical calculation parameters, the total amount of gas emitted from the longwall face exposed from 0 to t is

$$Q_{\mathrm{b}}' = \frac{h_c}{3} \times \frac{s}{3} \times \frac{l_0}{300} \int_0^t \left(\alpha e^{-\beta t} + \gamma\right) \mathrm{d}t.$$

$$(25)$$

By integrating t in equation (25), we have

$$Q_{\mathrm{b}}' = \frac{h_c s l_0}{2700}\left[\frac{\alpha}{\beta}\left(1 - e^{-\beta t}\right) + \gamma t\right],$$

$$(26)$$

and the amount of coal wall emissions per unit time is described as

$$Q_{\mathrm{b}} = \frac{h_c s l_0}{2700}\left[\frac{\alpha}{t\beta}\left(1 - e^{-\beta t}\right) + \gamma\right],$$

$$(27)$$

where s is the top support length of the hydraulic support and t is the exposure time of the longwall face, $t = 2l_0/v_c + t_0$ and t_0 is the clearance time of coal cutting.

4. Field Validation of Prediction Models

4.1. Gas Detection Location and Statistical Method for Gas Emission. Wangjialing 12322 working face strike length is 1228 m, inclined length is 310 m, and coal seam inclination is 2–7°. The coal seam is stable, the coal thickness is 5.90–6.45 m, the average is 6.2 m, the working face actually enters 8 knives every day, and the ruler is 6.4 m.

Figure 11 presents the layout of the gas monitoring probe in the coal mining face. The three probes are arranged in the lower corner (T_3), upper corner (T_1), and return air roadway (T_2), respectively. As the working face moves forward, the position of the probe moves correspondingly, yet the relative position remains unchanged.

(1) Calculation of gas emission Q_{b} from the coal wall:

① Calculation of gas emission $Q_{\mathrm{b}1}$ from the coal wall of the air inlet roadway: $Q_{\mathrm{b}1}$ can be calculated as follows:

$$Q_{\mathrm{b}1} = C_{31}q_{31},$$

$$(28)$$

where $Q_{\mathrm{b}1}$ is the gas emission from the coal wall of the air intake roadway, m³/min, C_{31} is the gas concentration observed by probe T_3 during the preparation process, %, and Q_{31} is the air volume observed by probe T_3 during the preparation process, m³/min.

② Calculation of gas emission quantity $Q_{\mathrm{b}2}$ from the coal wall of the mining face: $Q_{\mathrm{b}2}$ is determined based on the observation values of probe T_1 and T_3 during the preparation process:

$$Q_{\mathrm{b}2} = (C_{11}q_{11} - C_{31}q_{31}) - Q_{\mathrm{K}},$$

$$(29)$$

where $Q_{\mathrm{b}2}$ is the gas emission from the coal wall, m³/min, C_{11} is the gas concentration observed by probe T_1 during the preparation process, %, Q_{11} is the air volume observed by probe T_1 during the preparation process, m³/min, and Q_{K} is the gas emission from the goaf, m³/min. Note that Q_{K} is 0 when the goaf is not formed in the early stage of mining.

③ Calculation of gas emission $Q_{\mathrm{b}3}$ from the coal wall of the return air roadway: at the early stage of mining and prior to the formation of the goaf, $Q_{\mathrm{b}3}$ is determined based on the observation values of probes T_1 and T_2:

$$Q_{b3} = C_{23}q_1 - C_{13}q_1,$$

$$(30)$$

where $Q_{\mathrm{b}3}$ is the gas emission from the coal wall of the return air roadway, m³/min, C_{23} is the gas concentration observed by probe T_2 during the preparation process at the initial stage of mining, %, C_{13} is the gas concentration observed by probe T_1 during the preparation process at the initial stage of mining, %, and Q_1 is the air volume observed in the return air roadway during the initial preparation process of mining, m³/min.

(2) Calculation of gas emission Q_{L} during coal mining: Q_{L} can be calculated as follows:

$$Q_{\mathrm{L}} = q_2 \Delta C_1,$$

$$(31)$$

where Q_{L} is the gas emission from coal caving, m³/min, ΔC_1 is the gas concentration difference observed by probe T_1 during the coal mining and preparation processes, %, and Q_2 is the air volume of the mining face, m³/min.

(3) Calculation of gas emission Q_{K} in the goaf:

Under normal gas geological conditions, the difference between the total amount of gas emission observed by probe T_1 before and after the formation of the goaf is equal to the amount of gas emission Q_{K}:

$$Q_{\mathrm{K}} = C_{12}q_{12} - C_{13}q_{13},$$

$$(32)$$

where Q_{K} is the gas emission from the goaf, m³/min, C_{12} is the gas concentration observed by probe T_1 during the post-goaf formation coal mining process,
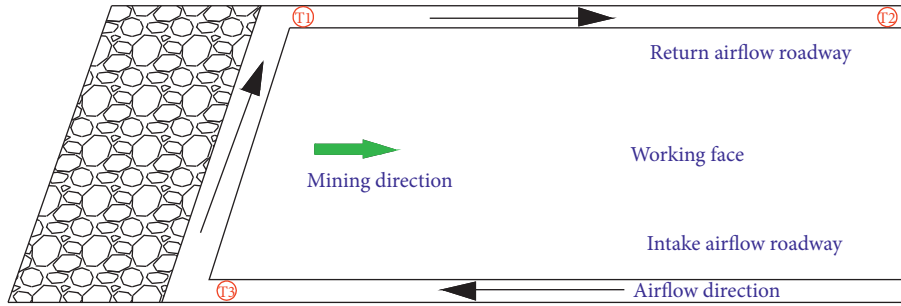
FIGURE 11: Layout of the gas probe in the coal mining face.

TABLE 3: Error ratio of field data to model calculations.

Time	Gas source	Field measurement (m³/min)	Model prediction (m³/min)	Error (%)
Early July	Coal wall	2.09	2.22	6.22
	Drop coal	3.03	3.21	5.94
	Goaf	1.01	1.10	8.91
	Total	6.13	6.53	6.53
Mid August	Coal wall	2.20	2.36	7.27
	Drop coal	3.15	3.35	6.35
	Goaf	1.14	1.24	8.77
	Total	6.49	6.95	7.09
Mid September	Coal wall	2.23	2.34	4.93
	Drop coal	3.06	3.30	7.84
	Goaf	1.17	1.21	3.42
	Total	6.46	6.85	6.04

%, Q_{12} is the air volume observed by probe T_1 during the post-goaf formation coal mining process, m³/min, and Q_{13} is the air volume observed by probe T_1 during the coal mining process prior to the formation of the goaf, m³/min.

4.2. Comparison of Field Measurements and Model Prediction Results. The field measured gas emissions were obtained via data from the gas monitoring probe in the 12322 working face during early July, mid August and mid September, 2019. The data in the nonproduction period were eliminated. The proposed prediction model, based on equations (14), (18), (23), and (27), was employed to derive the predicted gas emission results using the relevant parameters of the 12322 working face in Wangjialing mine.

Table 3 compares the field measurements and model predictions. The comparison and verification of the field data statistics and model calculation results are applied to determine a total emission error of 6.04–7.09%, coal wall emission prediction error of 4.93–7.27%, coal caving emission prediction error of 5.94–7.84%, goaf prediction error of 3.42–8.91%, and a gas emission prediction error from all sources lower than 10%. This indicates the strong reliability and accuracy of the gas emission dynamic prediction model.

5. Discussion

With a focus on the fully mechanized top coal caving mining face and coal particle size, a key factor affecting the gas emission, this paper tests the coal particle size distribution in a fully mechanized top coal caving mining face. Variations in the coal gas emission intensity are investigated, and the dynamic prediction model of multisource gas emissions in a fully mechanized top coal caving mining is further constructed.

At present, there are no fully developed methodologies for the measurement of coal particle size in coal mining faces. In the current paper, we propose image recognition technology to identify the coal particle size, with the ability to reflect the coal particle size distribution to a certain extent. However, the proposed method faces several limitations. For example, the large number of samples required to support the method reduces its applicability, and two-dimensional surface image recognition cannot fully characterize the spatial distribution of coal particle size.

We employ numerical simulations to evaluate the coal gas emission intensity, and the results provide a basis for the establishment of the subsequent model. However, due to the simplification of the actual conditions in the numerical simulation, the calculation results still differ to those from the actual situation. In order to solve this problem, we performed the further optimization of the existing results by means of physical experiments, improving the reliability and accuracy of the results.

Unlike existing prediction models, the proposed dynamic prediction model of multisource gas emissions for fully mechanized top coal caving mining takes full account of the particle size of coal and the dynamic time effect of gas

emissions, making it more suitable for real applications. Then, we verify the prediction model using field tests and compare the differences between the field measurements and model prediction results.

6. Conclusion

(1) The particle size distribution range of mined coal is observed to be more dispersed, with a higher proportion of small- and large-sized particles compared to the particle size distribution of caving coal. These differences may be related to the distinct coal breaking methods.

(2) The smaller the coal particle size, the faster the gas emission. The gas in 0–5 mm coal particles is essentially desorbed within 10 min, while the desorption ratio of the $\geq$ 20–60 mm coal particles is very low during the initial 30 min.

(3) The comprehensive emission intensity of coal mining and coal caving in the Wangjialing coal mine can be described with an exponential function. The initial emission intensity of coal mining exceeds that of coal caving, yet the attenuation laws of the two processes are essentially equal within 30 min.

(4) According to the research results of coal particle size distribution characteristics and gas desorption law, through mathematical derivation, the prediction models of gas emission from mining coal, caving coal, goaf, and coal wall are established, respectively.

(5) Through on-site gas concentration monitoring and calculation, the prediction results of gas emission from various sources are verified in early July, mid August, and mid September, and the error between the predicted results and the field data is within a reasonable range.

Data Availability

The data used to support the findings of this study are available from the corresponding author upon request.

Conflicts of Interest

The authors declare that they have no conflicts of interest.

Acknowledgments

References

[1] T. Liu, B. Lin, W. Yang, T. Liu, and C. Zhai, "An integrated technology for gas control and green mining in deep mines based on ultra-thin seam mining," *Environmental Earth Sciences*, vol. 76, no. 6, pp. 243–259, 2017.

[2] K. Wang, J. Zang, G. Wang, and A. Zhou, "Anisotropic permeability evolution of coal with effective stress variation and gas sorption: model development and analysis," *International Journal of Coal Geology*, vol. 130, pp. 53–65, 2014.

[3] Z. Pan, Y. Ma, L. D. Connell, D. I. Down, and M. Camilleri, "Measuring anisotropic permeability using a cubic shale sample in a triaxial cell," *Journal of Natural Gas Science and Engineering*, vol. 26, pp. 336–344, 2015.

[4] D. P. Greedya, "Geological controls on the formation and distribution of gas in British coal measure strata," *International Journal of Coal Geology*, vol. 10, no. 1, pp. 1–31, 1988.

[5] L. Qin, P. Wang, S. G. Li, H. F. Lin, R. wang, and C. Mao, "Gas adsorption capacity changes in coals of different ranks after liquid nitrogen freezing," *Fuel*, vol. 292, Article ID 120404, 2021.

[6] D. Dong, "Mine gas emission prediction based on Gaussian process model," *Procedia Engineering*, vol. 45, no. 2, pp. 334–338, 2012.

[7] L. Chen, E. Wang, J. Feng, X. Kong, X. Li, and Z. Zhang, "A dynamic gas emission prediction model at the heading face and its engineering application," *Journal of Natural Gas Science and Engineering*, vol. 30, pp. 228–236, 2016.

[8] P. Booth, H. Brown, J. Nemcik, and R. Ting, "Spatial context in the calculation of gas emissions for underground coal mines," *International Journal of Mining Science and Technology*, vol. 27, no. 5, pp. 787–794, 2017.

[9] Y. Zeng and C. f. Wu, "Research on fuzzy fractal neural network for prediction of mine gas emission," *Coal Science & Technology Magazine*, vol. 32, no. 1, pp. 62–65, 2004.

[10] L. Qin, S. Li, C. Zhai et al., "Changes in the pore structure of lignite after repeated cycles of liquid nitrogen freezing as determined by nitrogen adsorption and mercury intrusion," *Fuel*, vol. 267, Article ID 117214, 2020.

[11] S. L. Shi and A. Y. Wu, "Application of GM (1, 1) and line regression for predicting amount of mine gas emission in coalmine," *Meitan Xuebao/Journal of the China Coal Society*, vol. 33, no. 4, pp. 415–418, 2008.

[12] T. Wen, X. Sun, X. Kong, and H. B. Tian, "Research on prediction of gas emission quantity with sub sources basing on PSOBP-AdaBoost," *China Safety Science Journal*, vol. 25, no. 6, pp. 94–98, 2016.

[13] M. Deng, G. S. Zhang, and Q. H. Chen, "Forecast of coal and gas outburst based on time series of gas concentration," *Journal of China Coal Society*, vol. 35, no. 6, pp. 260–263, 2010.

[14] J. H. Fu and Y. P. Cheng, "Situation of coal and gas outburst in China and control counter measures," *Journal of Mining &Safety Engineering*, vol. 24, no. 3, pp. 253–259, 2007.

[15] H. Fu, S.. Xie, Y. S. Xu, and Z. C. Chen, "Gas emission dynamic prediction model of coal mine based on ACC-ENN algorithm," *Journal of China Coal Society*, vol. 39, no. 7, pp. 1297–1301, 2014.

[16] P. Liu, H. Z. Wei, and J. B. Jing, "Predicting technology of gas emission quantity in coal mine based on enhanced CART regression algorithm," *Coal Science and Technology*, vol. 47, no. 11, pp. 116–122, 2019.

[17] H. J. Zhang, L. Zhang, Y. Q. Liu, and J. H. Sun, "Prediction of gas emission volume from driving face based on seepage mechanics," *Coal Science and Technology*, vol. 43, no. 8, pp. 82–86, 2015.

[18] F. Lv, B. Liang, W. J. Sun, and Y. Wang, "Gas emission quantity prediction of working face based on principal component regression analysis method," *Journal of China Coal Society*, vol. 27, no. 1, pp. 113–116, 2012.

[19] H. Q. Zhu, W. J. Chang, and B. Zhang, "Different source gas emission prediction model of working face based on BP

artificial neural network and its application," *Journal of China Coal Society*, vol. 32, no. 5, pp. 504–508, 2007.

[20] A. Y. Wu, Y. L. Tian, Y. Song, and L. W. He, "Application of the grey system theory for predicting the amount of mine gas emission in coal mine," *China Coal Society*, vol. 30, no. 5, pp. 589–592, 2005.

[21] F. Du and K. Wang, "Unstable failure of gas-bearing coal-rock combination bodies: insights from physical experiments and numerical simulations," *Process Safety and Environmental Protection*, vol. 129, pp. 264–279, 2019.

[22] W. Zhao, K. Wang, S. Liu et al., "Asynchronous difference in dynamic characteristics of adsorption swelling and mechanical compression of coal: modeling and experiments," *International Journal of Rock Mechanics and Mining Sciences*, vol. 135, Article ID 104498, 2020.

[23] Y. Q. Tao, J. Xu, and S. C. Li, "Predict gas emission quantity of mining coal face with improved grey Markov model," *MeitanXuebao/Journal of the China Coal Society*, vol. 32, no. 4, pp. 391–395, 2007.

[24] F. Du, K. Wang, X. Zhang, C. Xin, L. Shu, and G. Wang, "Experimental study of coal-gas outburst: insights from coal-rock structure, gas pressure and adsorptivity," *Natural Resources Research*, vol. 29, no. 4, pp. 2481–2493, 2020.

[25] Y. Yang, Y. Mu, and H. Qin, "Research on time series characteristics of gas concentration at working face and application of them to early warning," *China Safety Science Journal*, vol. 3, pp. 120–125, 2018.

[26] S. Zhu, Y. Wang, and L. Wei, "Gas monitoring warning signal identifcation based on time series similarity measure," *Journal of China University of Mining and Technology*, vol. 41, no. 3, pp. 474–480, 2012.

[27] L. Qin, P. Wang, S. Li et al., "Gas adsorption capacity of coal frozen with liquid nitrogen and variations in the proportions of the organic functional groups on the coal after freezing," *Energy & Fuels*, vol. 35, no. 2, pp. 1404–1413, 2021.

[28] H. Wang, X. Fang, F. Du et al., "Three-dimensional distribution and oxidation degree analysis of coal gangue dump fire area: a case study," *The Science of the Total Environment*, vol. 772, Article ID 145606, 2021.

[29] W. Zhao, K. Wang, L. Wang et al., "Influence of matrix size and pore damage path on the size dependence of gas adsorption capacity of coal," *Fuel*, vol. 283, Article ID 119289, 2021.

[30] C. W. Li, H. L. Xue, and W. B. Liu, "Experimental study on gas diffusion in coal under stress," *Journal of China Coal Society*, vol. 43, no. 3, pp. 717–723, 2018.

[31] Z. Q. Kang, X. Li, W. Li, and J. Zhao, "Experimental research on the correlation between coal structure and methane adsorption/desorption law and its enlightenment," *Journal of China Coal Society*, vol. 43, no. 5, pp. 1400–1407, 2018.

[32] Y. W. Liu, J. P. Wei, Z. G. He, and M. J. Liu, "Influence rules and mechanisms of temperature on dynamic process of gas diffusion from coal particles," *Journal of China Coal Society*, vol. 38, no. S1, pp. 100–105, 2013.